Shahid Chamran University of Ahvaz

Iranian Association of Electrical and Electronics Engineers

Journal of Applied Research in Electrical Engineering

E-ISSN: 2783-2864
P-ISSN: 2717-414X
Homepage: https://jaree.scu.ac.ir/

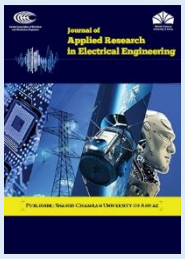

Research Article

Partial Discharge Pattern Recognition in GIS Using External UHF Sensor

Reza Rostaminia*, Mehdi Vakilian, and Keyvan Firouzi

Electrical Engineering Department and Centre of Excellence in Power System Management and Control, Sharif University of Technology, Tehran 1458889694, Iran

** Corresponding Author: Reza_rostaminia@ee.sharif.edu*

Abstract: Partial Discharge (PD) measurement is one of the best solutions for condition assessment of Gas Insulated Switchgears (GISs). For having Condition-based maintenance of GIS, online PD monitoring is of great importance. For this aim, Ultra High Frequency (UHF) PD sensors should be installed inside the GIS during the installation. However, in most installed GISs in industries, the internal UHF PD sensors are not installed. In this paper, a new method for online defect type recognition according to external UHF PD sensors and based on the time-frequency representation of PD signal is proposed. In this case, four artificial defect types named protrusion on the main conductor, protrusion on the enclosure, free moving metal particle, and metal particle on spacer are implanted inside the 132 kV L-Shaped structure of one phase in enclosure GIS. The signal energy at each level of the decomposed signal by Discrete Wavelet Transform (DWT) is applied for features of each defect type. The trends of signal energy variations at each frequency range of signal are applied for discriminating between each defect type. The Deep Feed Forward Network (DFFN) classifier is applied for PD pattern recognition. The results show the benefits and simplicity of the proposed method for PD signal classification, independent from the position of the PD sensor, especially in the case of online PD monitoring of GIS.

Keywords: Gas insulated switchgear (GIS), partial discharge (PD), ultrahigh frequency (UHF) measurements, pattern recognition, time-frequency representation.

Article history
Received 30 March 2022; Revised 31 October 2022; Accepted 06 December 2022; Published online 29 March 2023.

How to cite this article
R. Rostaminia, M. Vakilian, and K. Firouzi, "Partial discharge pattern recognition in GIS using external UHF sensor," *J. Appl. Res. Electr. Eng.*, vol. 2, no. 1, pp. 75-86, 2023. DOI: 10.22055/jaree.2022.40395.1054

Check for updates

1. INTRODUCTION

Partial Discharge (PD) monitoring is one of the most useful method for detecting insulation defects in the early stages of development in Gas Insulated Switchgears (GIS). PD occurrence can be monitored via different methods such as conventional electrical IEC 60270 method [1]-[2], gas analysis method [3], ultrasonic method [4], optical detection method [5] and electromagnetic method in GIS [6]. The conventional electrical IEC 60270 technique is one the most popular method for PD detection in GIS [7]. In this method, the PD apparent charge can be measured via a coupling device. The main advantage of this method is quantifying the discharge level in pico-colomb range [8]. However, the main disadvantage of using the IEC 60270 method is needing to use coupling capacitor device which imposed some restrictions, especially in at-site testing [9]. The ratio of coupling capacitor value to the test object equivalent capacitance has great impact on measurement sensitivity. This is in great importance especially in case of at-site GIS testing with long length, since applying large value of coupling capacitor can be difficult. Furthermore, the other disadvantage of this method is its sensitivity to internal and external interferences [10].

The acoustic detection method can be employed for measuring the acoustic waves generated by PD within the GIS. The advantage of this method is its well quantification of the PD level and the risk assessment during online operation [11]. However, the main disadvantage of this method is the high uncertainty in the obtained results due to existence of noise and electric interferences [12]. The optical spectrum of measured signal via optical sensors installed in a GIS system varies due to presence of contaminants or surface roughness. This is another way for partial discharge detection [13]. However, the application of optical detection method is restricted due to limitation in accessing the GIS interior

design information. Also, some components of GIS such as solid spacers and cable or cable sealing ends can be unchecked during PD measurement via this method. Another method to detect occurrence of PD within the GIS is by analysis of by-products of SF6 decomposition [14]. With quantifying the decomposed components of SF6, the level of insulation degradation and the type of defects can be reached [15]. One of the dis advantage of this method is that it should be performed off-line and the generated by-products due to decomposition of SF6 is time-consuming process. Also, some defect types, such as: occurrence of voids within the epoxy insulating material of GIS spacer or another insulator can be undetectable with this method.

Ultra High Frequency (UHF) sensors can be applied to measure the radiated electromagnetic waves due to PD occurrence within the GIS. The internal and external UHF sensors can be exploited for measuring PD in GIS [16-17].

Unlike the preferences of internal sensors compared to the external ones due to better sensitivity and noise immunity features, however in most GIS in service, these internal sensors have not been installed. Accordingly, the external sensors can be applied for PD monitoring. One of the main challenges in UHF PD monitoring systems of GIS is distinguishing the type of defects. The recorded PD wave shape can be changed with defect type within the GIS [18]. However, some parameters such as the distance between the measuring sensor and the defect [18], the propagation path due to configuration of GIS such as L-Shaped and T-Shaped structure, spacer thickness and disconnectors [19-21], can influence on PD measured wave shape. Recorded PD data can be represented via Phase-Resolved Partial Discharge (PRPD) or Time-Resolved pattern. In PRPD pattern, usually the PD magnitude in (mV), phase angle of applied voltage at the time of PD occurrence and the number of PD occurred are represented [22]. In time-resolved patterns of PD wave shape of PD signal is recorded and the type of defects can be distinguished due to the fact that each defect can result in specified PD wave shape. Although the efficiency of PRPD pattern analysis in recognition of defect type is proven but, one of its main challenge is occurring two or more defects simultaneously within the GIS. In this case, the segregation of patterns can be difficult [23]. In some works, the time-domain pattern is applied for PD defect recognition [24]. In [25], the envelope detection circuit (based on a mathematical method for waveform estimation) is applied to extract the time-domain signal. Then, the noise reduction technique based on wavelet is used to extract the de-noised PD wave shape. The pattern classification is performed using the “back propagation neural network” (BPNN). In [26], the Damper-Shafer (DS) theory is established for feature extraction from both PRPD and time-domain pattern of PD within 126 kV GIS. In [27], the Convolutional Neural Network (CNN) is used to classify the extracted features from time-frequency representation of the signal. In [28], the gray scale image for time-frequency representation of PD signal using S-Transform is applied to extract features from five regions of Transverse Electromagnetic (TE) mode. The extracted features based on low order moments and J-criterion are feed to three classification methods, named Support Vector Machine (SVM), K-Nearest Neighbor (KNN) and particle swarm optimized Extreme Learning Machine (ELM). Finally, it is shown that the ELM has a better performance not only in respect to the classification accuracy, but also in the learning process and the test speeds.

However, in most of the recent works for pattern recognition of PDs in GIS, the employed data are related to the recorded PD data from the UHF sensors installed inside the GIS enclosure. Also, in some works, the proposed methods are complex and in practice, their implementation is difficult. Since the internal UHF PD sensors have not been installed in most of GIS under operations in the electric power industries around the world, the only way for UHF PD online monitoring is the application of the external UHF sensor. Thus, the authors propose a method for pattern recognition of recorded PD data captured by an external UHF PD sensor installed on a sample GIS busbar. Therefore, the L-shape arrangement of GIS sample busbar with artificial embedded defects are applied for the PD measurements. Then, the time-frequency representation of PD signal from wavelet transform is used to identify the features that can discriminate among the various defects. It is shown the energy of the signals in various frequency ranges are different for different type of defects. Finally, the DFNN classifier is applied for classification of the detected PD defect types.

2. EXPERIMENTAL SETUP

The L-shape structure of gas insulated busbar is selected for implanting four artificial defects and it is shown in **Fig. 1** This L-shape arrangement of GIS model is constructed with one phase conductor in enclosure and the rated voltage for this model is 132 kV. The absolute SF6 gas pressure in this L-shape model is 4 bar. This L-shape structure is connected to oil-insulated busbar which is terminated with an air-insulated bushing to apply high voltage as shown in Fig. 1.

Two inspection windows are considered at the end of the straight part and the L-shape part of this model. These windows are designed in such a way that a UHF PD sensors can be placed in them for capturing the PD data. The UHF PD sensors installation location is shown in Fig. 2.

Two inspection windows are considered at the end of the straight part and the L-shape part of this model. These windows are designed in such a way that a UHF PD sensors can be placed in them for capturing the PD data. The UHF PD sensors installation location is shown in Fig. 2.

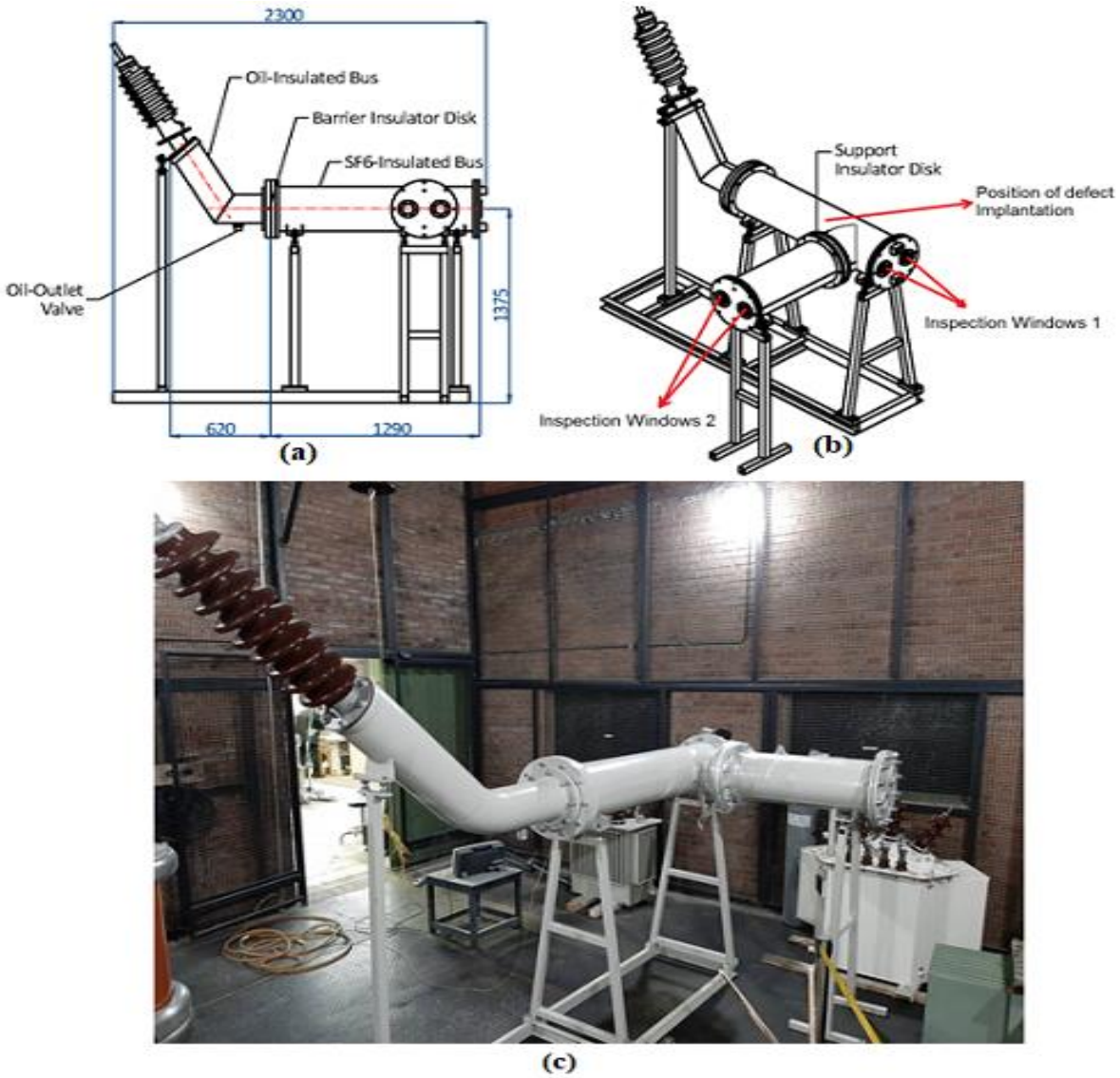

Fig. 1: The L-shape arrangements of GIS experimental busbar, (a) side view (b) 3D view (c) installed in HV laboratory of Electrical Engineering Department, Sharif University of Technology.

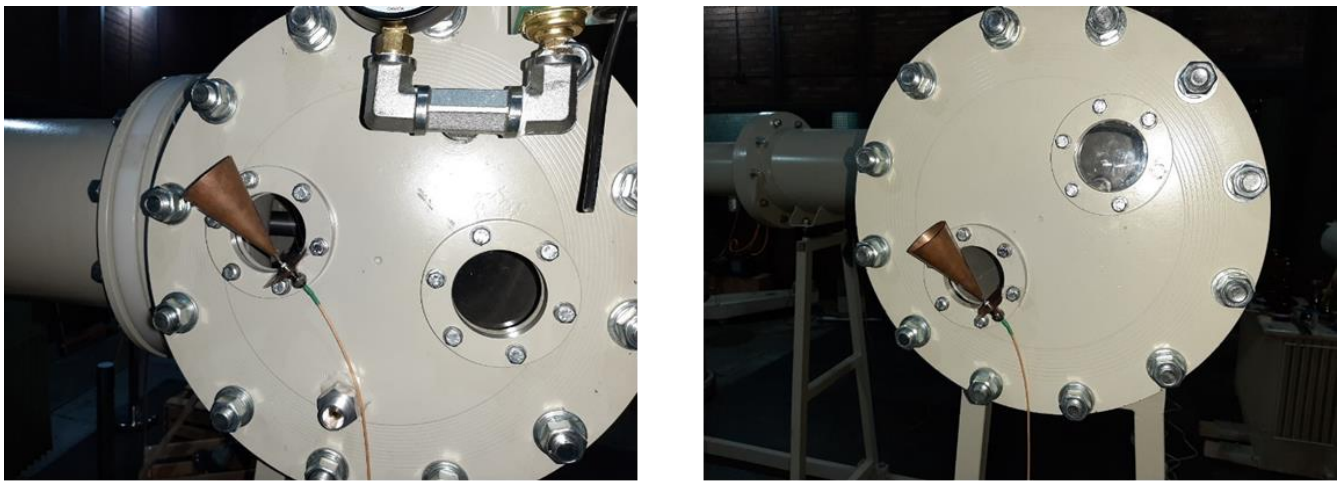

(a) (b)

Fig. 2: External UHF PD Sensor installation on observing window of L-Shape GIS model, (a) UHF PD sensor 1, (b) UHF PD sensor 2.

Two types of UHF PD sensors, called externally and internally connected UHF sensors, can be applied for PD measurements in GIS. Although the internally connected PD sensors are more sensitive than the externally connected ones, but in most energized GIS in industries, the internally PD sensors have not been installed inside the GIS. Accordingly, the condition monitoring and PD measurements can just only be performed with externally connected PD sensors. Various types of externally UHF antenna such as bio-conical log periodic antenna, loop antenna, horn antenna, dipole antenna and planar antenna can be applied for PD measurements [29]-[33]. The external PD sensors can be applied both at the bush type spacers (spacers with no metallic coverage) and at the inspecting windows of disconnect and earthing switches. All the above mentioned antennas have features and quality that can be chosen for reaching the specified goal. As an example, horn antenna have the most sensitivity at higher frequencies which the dipole and log-periodic antenna have better frequency response at lower range of frequencies. However, there are some restrictions for using these antennas due to the position where they should be applied. In this case, the dipole antenna can have the best performance since be directly connected to the flanges.

In this study, the aim is discriminating the difference between various types of defects due to time-domain measured PD signals, the horn antenna is applied for measuring UHF PD signals. The frequency response of the horn antenna UHF PD sensor is presented in Fig. 3.

Four typical defects named: 1- metal protrusions on main HV conductor, 2- metal protrusions on grounded enclosure, 3- free moving metal particle and 4- A metal particle on epoxy resin insulating material of GIS spacer are implemented in to this GIS busbar system as artificial defects (Fig. 4). The

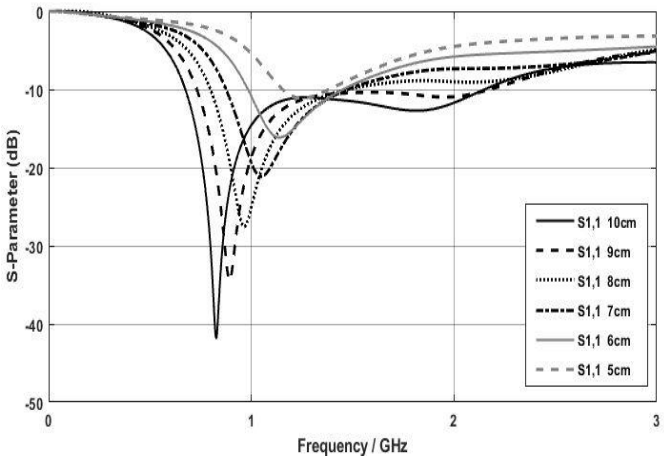

Fig. 3: Frequency Response of horn antenna.

defects number 1 and 2 are created via a 2 cm sharp point needle, soldering it to the main HV conductor and enclosure of the model, respectively (Fig. 4a, and b). While, defect No. 3 is implanted in this experimental GIS system using some little free moving metal particles; each of them 1 mm in length (Fig. 4c). A 2 cm length of metal wire is located in a fixed position on the surface of epoxy insulating material of the GIS system spacer; between the core HV conductor and the grounded enclosure, to represent the defect No. 4 (as shown in Fig. 4d).

The main circuit and the experimental test setup for measurement of electromagnetic radiation due to the PD occurrence are depicted in Fig. 5. The positions of implanted the defects are in the straight section of the GIS busbar model; as shown in Fig. 1.

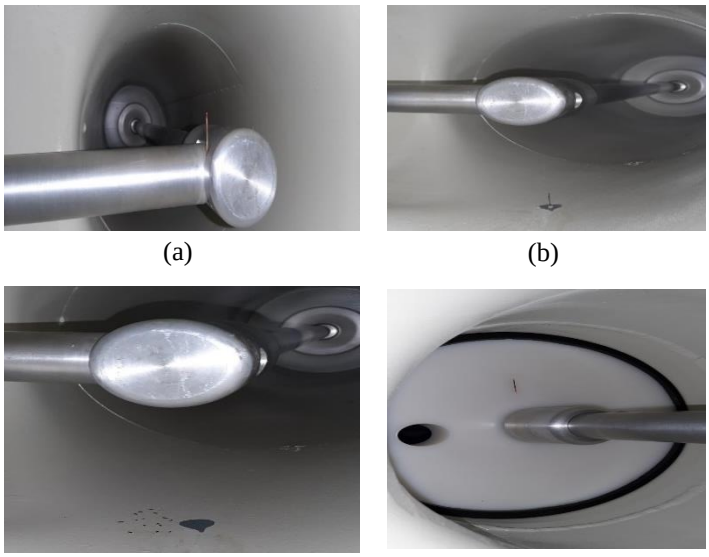

(a) (b)

(c) (d)

Fig. 4: Four artificial defect types, as applied to the experimental L-shaped GIS busbar, (a) protrusion on the main HV conductor, (b) protrusion on the enclosure of GIS, (c) free moving metal particle, (d) metal on epoxy resin of GIS spacer.

(a)

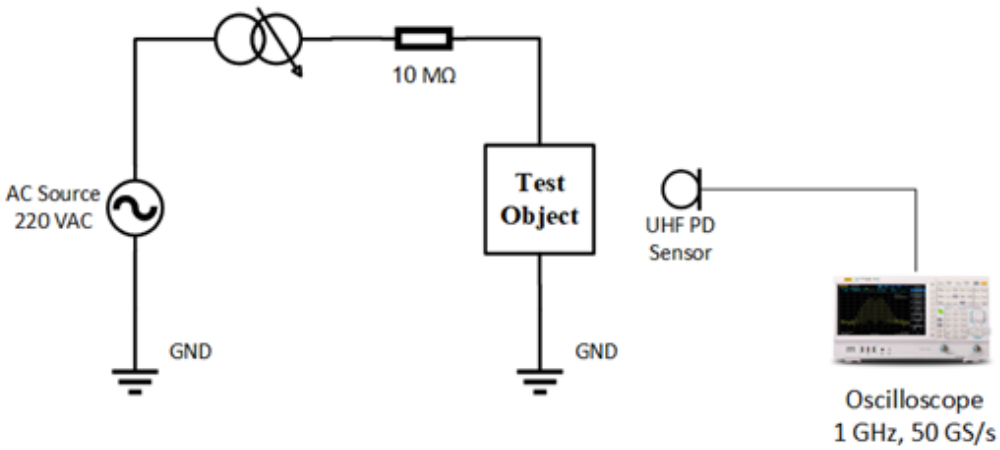

(b)

Fig. 5: (a) The test setup in the HV laboratory, and (b) the PD test circuit using UHF sensor.

3. DATA ACQUISITION

The recorded time-domain PD pulse for four defect types implanted in the L-shape GIS experimental model, using UHF sensor No. 1 are represented in Fig. 5. The magnitude of PD pulses are per-united based on the maximum measured value of PD for each defect by sensor No. 1. Each PD signal is recorded over 1100 time samples and each sample has a length of 0.02 ns.

As it can be seen the PD wave shape related to each defect have some differences compared to each other. It needs to be considered that these recorded data are based on the positioning of UHF PD sensors No. 1, which is just directly in line with defects implantation. In Fig. 6, the recorded time-domain PD wave shape are related to the four defect types, through the UHF PD sensor No. 2 measurement.

As it can be seen, there are significant differences between recorded PD signal waveform from sensor No. 1 and sensor No. 2. These differences are strongly related to the position of each measuring UHF PD sensor. Based on their positions, the radiations and reflections of electromagnetic PD waves on their ways to reach the UHF sensors can result in different time-domain PD recorded wave shapes. Since the PD sensor No. 1 is very close to the defect's position, the radiated electromagnetic PD waves are directly reached to this sensor. Therefore, the recorded PD data have less distortions and fluctuations. However, the recorded PD waveform by sensor No.2 contains a lot of fluctuations. The other important fact is that the amplitude of the recorded PD data strongly depends on the relative location of the defect and sensor position. It is obvious, that as the defect position is more close to the UHF PD sensor results in higher amplitude of measured PD. This is very important especially in case of using external PD sensor. Accordingly, the proposed method for defect type recognition is independent from PD magnitude and the amplitude of presented PD wave shape in Fig. 6 and Fig. 7 are per-united.

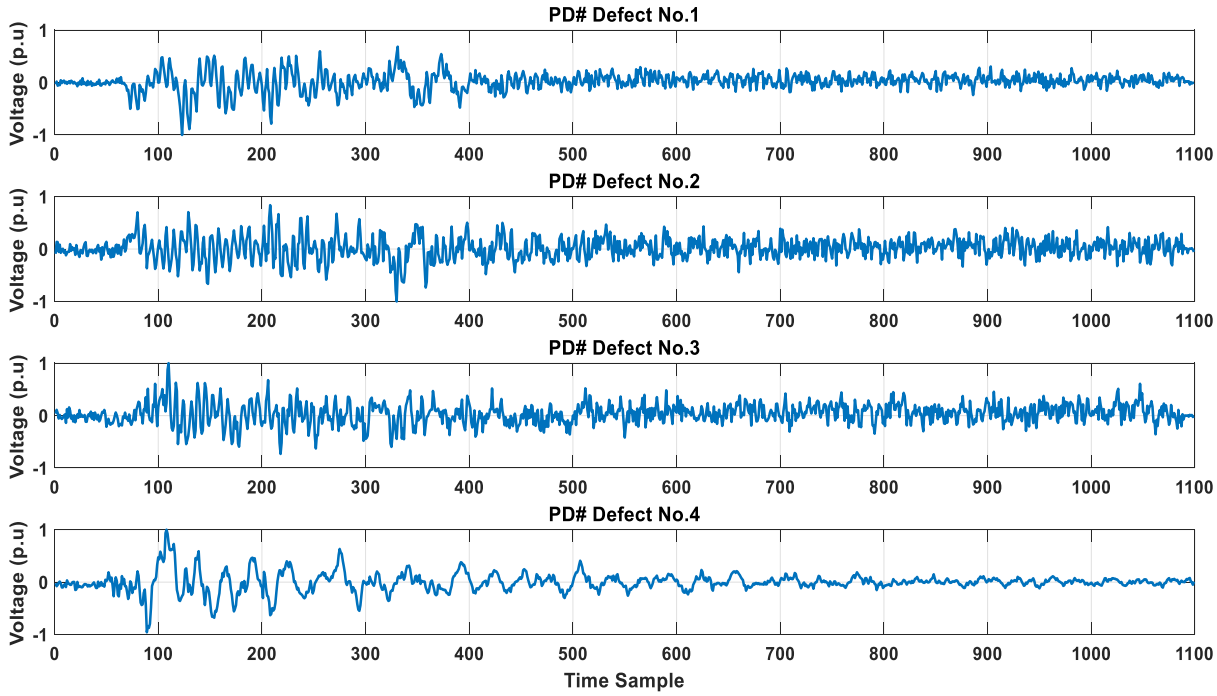

Fig. 6: PD time-domain signal measured by sensor No. 1 for the four different defect models.

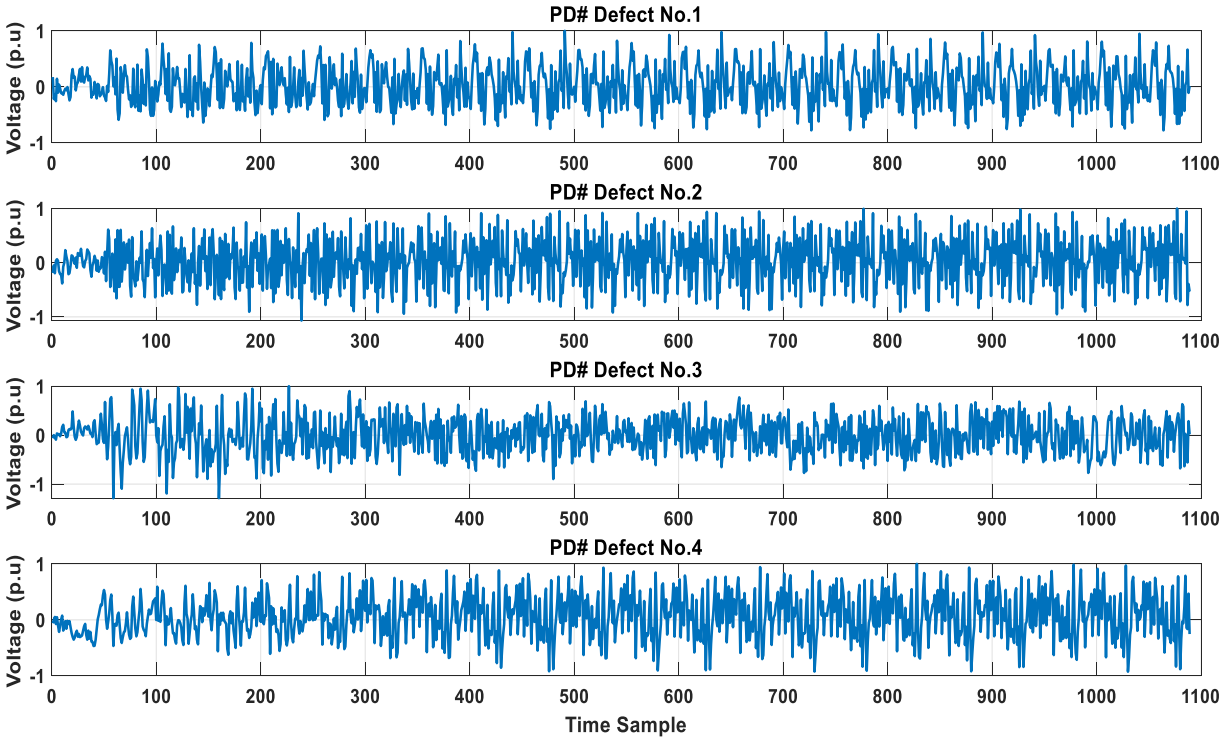

Fig. 7: PD time-domain signal measured by sensor No. 2 for four defect models.

4. Feature Extraction and Pattern Classification

As it can be seen from Fig. 5 and Fig. 6, the recorded PD data from one specific defect have considerable differences in their wave shape based on positioning of UHF PD sensor. Accordingly, some features related to their wave shape may have not enough capability for discrimination between each defect type. To solve this problem, the time-frequency representation of PD signal based on Discrete Wavelet Transform (DWT) is proposed in this paper.

4.1. Discrete Wavelet Transform

The Discrete Wavelet Transform (DWT) is a well-known choice for representing time- frequency representation of signals with lots of distortions. With selecting proper mother wavelet, a signal can be decomposed in different levels to some of its different frequency ranges at specific times. Based on decomposition level, the coefficient of similarity between

original signal wave and mother wavelet is represented in time- domain. The decomposition level of original signal wave strongly depends on frequency components of original signal. At each level of decomposition, a low-pass and high-pass filter is applied to the signal. The output of low-pass and high-pass filters are called the signal approximation and signal details, respectively.

The "db-4" is selected as mother wavelet for signal decomposition. The frequency range of recorded PD wave is restricted to 1 GHz due to limitation of frequency ranges of oscilloscope. Accordingly, three decomposition levels are selected and their related frequency ranges for "signal approximation" and "signal details" at each decomposed level of wavelet transform are shown in Fig. 8. At decomposition level 1 of PD signal, the approximation and details of the signal have the components with frequency ranges 0-0.5 GHz and 0.5 to 1 GHz, respectively. Also at decomposition level 2, the coefficients of the signal in approximation and details are in frequency ranges between 0-250 MHz and 250-500 MHz, respectively. Finally, at decomposition level 3, the approximation and details of signal have frequencies 0-125 MHz and 125-250 MHz, respectively.

In Fig. 9 and Fig. 10, the main PD signal wave and the approximation at level 3 and details at level 1, 2 and 3 of discrete wavelet transform for the four defect types of UHF sensor 1 and 2 are shown, respectively.

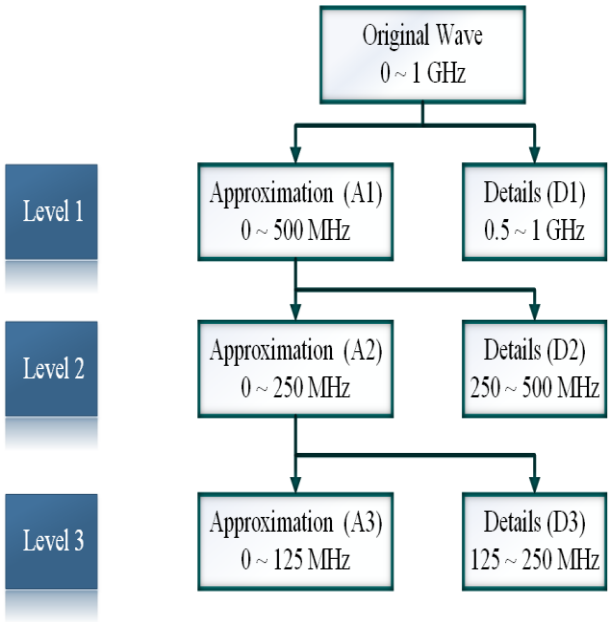

Fig. 8: The Discrete Wavelet Transform decomposition level applied to measured PD signal.

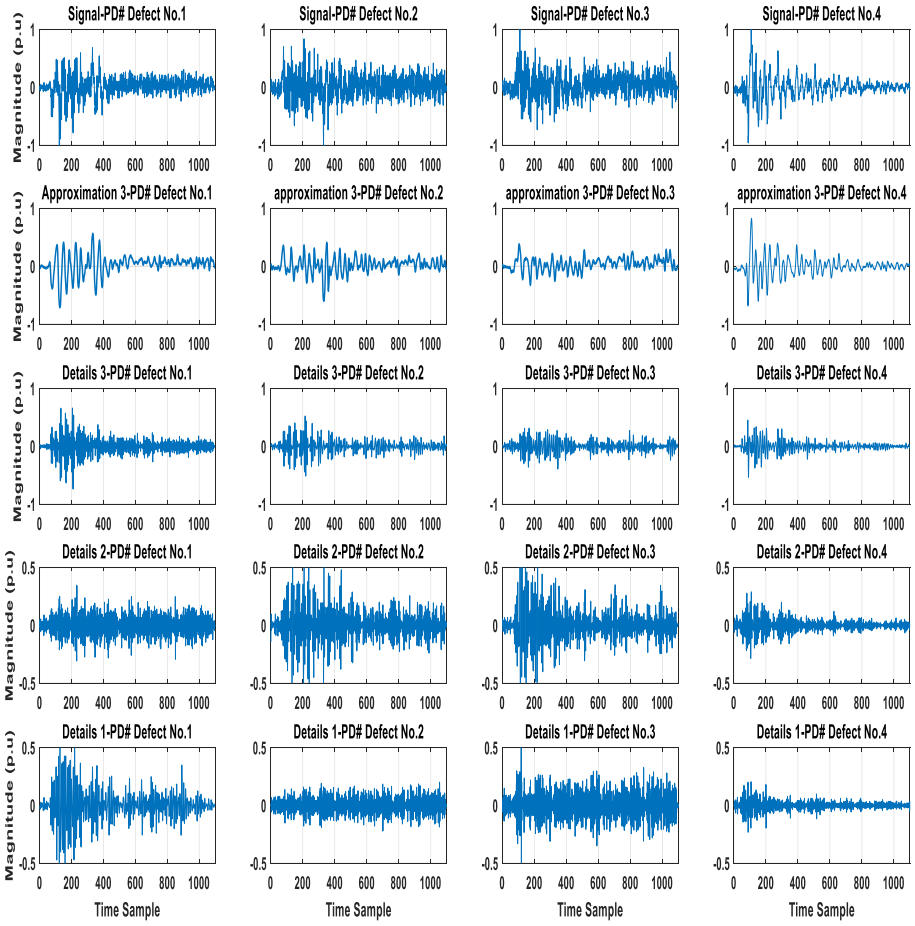

Fig. 9: The Main signal and the approximation and details of DWT for four defect types of UHF sensor 1.

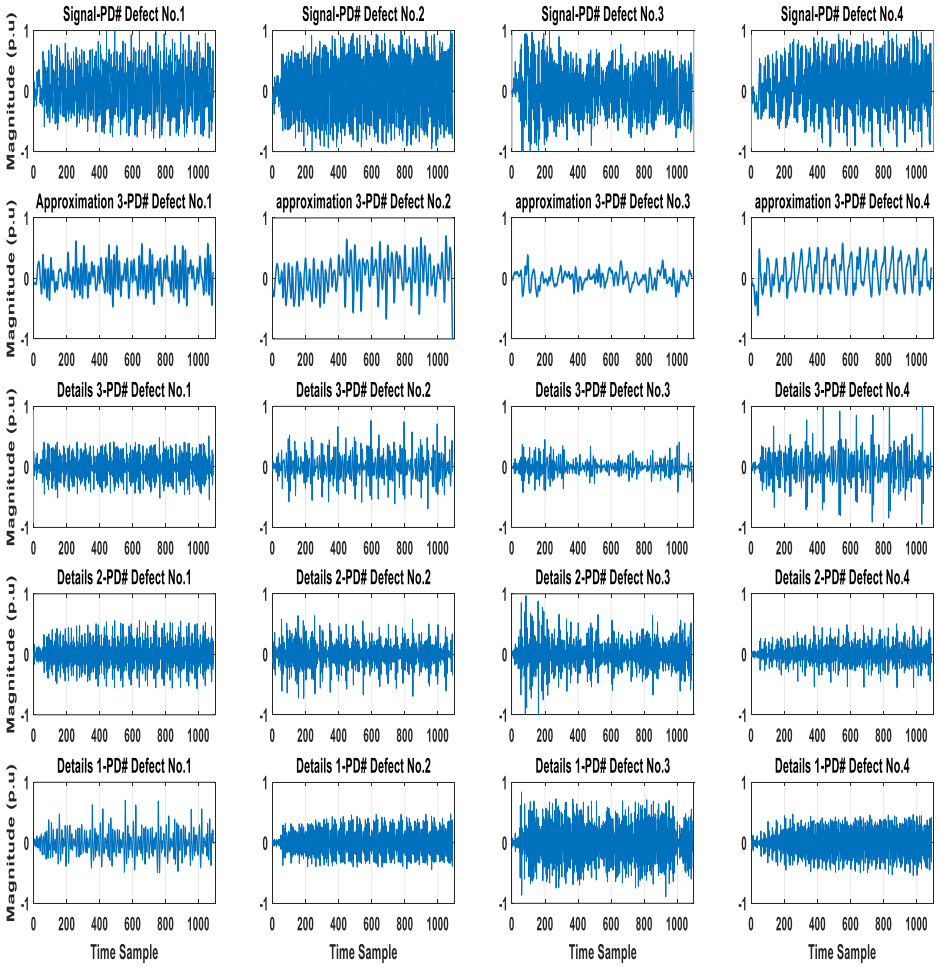

Fig. 10: The Main signal and the approximation and details of DWT for four defect types of UHF sensor 2.

Since the magnitude of PD pulse strongly depends on the distance of PD source and the UHF PD sensor, then the features extracted for pattern recognition should be independent of the PD pulse magnitude. Therefore, the magnitude of each PD pulse is presented in per unit, using its maximum as base. This is the main challenge for defect type identification based on time-domain PD pulse. In some past works time-domain PD data is employed for defect type identification, using pulse shape parameters such as the rise time, fall time, maximum amplitude, average amplitude and other parameters of PD signal [25-26]. However, due to presence of extensive distortions in each level of decomposition and also in main signal, the main wave shape features of PD signal are not proper for pattern recognition [27-33]. This is especially more critical for defects which are far from or are not in line with the PD sensor position [34]. Since, the fluctuations of PD pulse in different frequency ranges are different as it can be seen from Fig. 7 and Fig. 8, each defect type results in a specific radiated electromagnetic wave energies over some different frequency ranges. Accordingly, to solve the abovementioned problem, the signal's energy in each frequency ranges based on (1) is selected as its main feature for each defect type:

$$\text{Signal Energy} = \sqrt{\sum_{i=1}^{n} \left| a_i^2 \right|} \qquad (1)$$

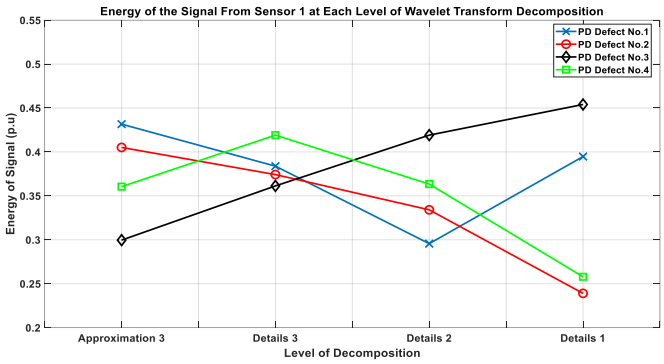

Fig. 11: Signal energy from sensor No. 1 at each level of WT decomposition (explained in Fig. 7).

where a_i is the coefficient of the signal at each level of wavelet transform decomposition and is the number of time sample or recorded PD signal.

The comparison of signal energies in different frequency ranges are depicted in Fig. 10 and Fig. 11 for the captured signals by sensors 1 and 2, respectively. As it can be seen from these figures, the trends of pulse energy variations in each frequency range differs due to the defect type of pulse origin. The pattern of these changes seems to be unique based on defect types and it is independent from positioning of UHF PD source.

In Fig. 10 and Fig. 11, for PD defect No. 1 the signal energy at approximation level 3 is maximum value among all the decomposition levels and the signal energy at details level 2 is the minimum value. However, the signal energy is increased in details 1 from details 2. For defect No. 2, the maximum and minimum amount of signal energies are related to the approximation 3 and details 1, respectively. The signal energy is decreased at each level of decomposition and the main energy of the signal is in frequency ranges between 0-125 MHz. For defect No. 3, the signal energy increased from approximation 3 to details 1. It can be seen the maximum energy of the signal corresponds to details 1 and frequency ranges between 0.5-1 GHz. However, for defect No. 4, the maximum and minimum energy of signal are in details 3 and details 1, respectively. In this type of defect, first the PD signal energy is increased from approximation 3 to details 3 and then the energy is decreased to details 1. The important point in investigation of signal energy at different range of frequency is that these trends of variations are related to the type of defects and they are independent from position of UHF PD sensor. These trends are presented in Table 1.

4.2. Deep Feed Forward Network (DFFN)

Artificial neural network is a well-known method for classification of different PD defect types [35]. In this case, the deep feed forward network is the most popular and simplest one in classification problems. In this paper, the feed forward neural network with three hidden layers are applied for PD defect type classification. As it can be seen in Fig. 12, the signal energy at approximation 3, details 3, details 2 and details 1 are selected as inputs of neural network.

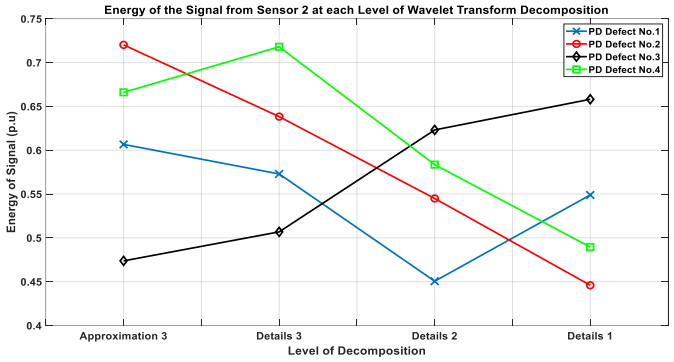

Fig. 12: Signal energy from sensor No. 2 at each level of WT decomposition (signal approximation level 3, and signal details levels 1, 2, and 3 as defined in Fig. 7).

Table 1: The signal energy variation trends at each level of decomposition.

	Signal Energy Variations			
	from Approximation 3 to Details 3	from Details 3 to Details 2	from Details 2 to Details 1	Pattern Code
PD Defect No.1	↘	↘	↗	(0,0,1)
PD Defect No.2	↘	↘	↘	(0,0,0)
PD Defect No.3	↗	↗	↗	(1,1,1)
PD Defect No.4	↗	↘	↘	(1,0,0)

At hidden layer 1, the comparison of signal energy between two adjacent levels of decomposition is done. Then, the rectified linear unit function is applied in hidden layer 2 to make the output of the signal between 0 and 1. In hidden layer 3, the outputs of compared energy of signal, based on values 0 and 1 are compared to each other for making pattern code. The created pattern code with the one presented in Table 1 result in type of defects classification. For training the Deep feed-forward network 200 recorded PD waveform for each type of defects are selected. Then, the 300 recorded data are applied to validate the proposed method for partial discharge pattern recognition. In Table 2, the misclassification matrices for the proposed PD pattern recognition method is presented.

As it can be seen in Table 2, the maximum and minimum Identification Percentage (IP) are for data related to defect No. 3 and defect No. 2, respectively. However, the average IP for the proposed PD pattern recognition is 94.5% and this means that the proposed methods especially for on-line PD monitoring of GIS is acceptable. It should be noted in the proposed method, there is no need to employ an internal UHF PD sensor be installed inside the GIS and also it is independent from the location of PD sensors.

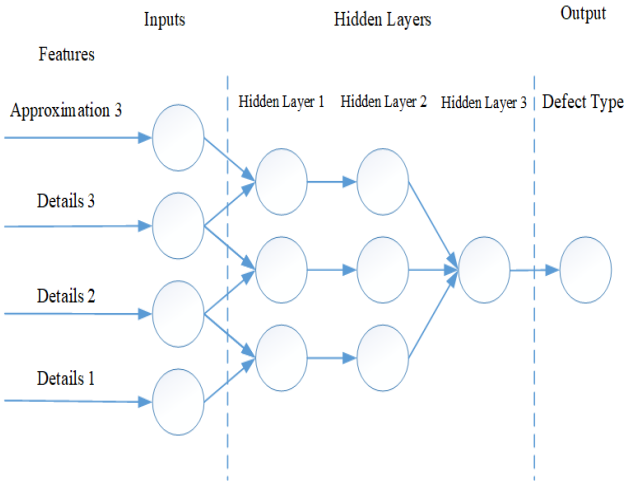

Fig. 13: The deep feed forward network classifier for PD pattern recognition.

Table 2: The misclassification matrices for the proposed PD pattern recognition method in GIS.

		Target Class			
		Defect 1	Defect 2	Defect 3	Defect 4
Output Class	Defect 1	282	15	3	6
	Defect 2	15	276	1	10
	Defect 3	1	0	291	2
	Defect 4	2	9	5	282
Correct Identification Percentage (IP%)		94 %	92 %	98 %	94 %
Total Accuracy		94.5 %			

5. Summary and Conclusion

Online partial discharge monitoring is one of the most important method to assess the condition of GIs. However, in most installed Gas insulated switchgears, the internal UHF PD sensors are not installed inside the GIS. In this paper, on-line partial discharge pattern recognition method is presented based on measured PD data from external UHF PD sensor. The time-frequency representation of signal from discrete wavelet transform is applied for feature extractions of each PD defect model. Four artificial defect models are implanted inside the 132 kV L-Shape GIS model. The feature extracted based on signal energy at each level of DWT decomposition are independent from positioning of UHF PD sensors. This is important when the UHF PD sensors are not installed inside the GIS busbar. Then, there would be just some few locations on GIS busbar which the external UHF PD sensors can be implanted. The trends in partial discharge signal energy variations in each level of DWT decomposition, present a significant potential for pattern recognition. By using the Deep Feed-Forward Network, the classification accuracy of the proposed method for PD pattern recognition is about 94.5 %.

Acknowledgement

Authors would like to thank Mr. Mohammad Bagher Souzanchi the managing director of Toskat Co., for providing an L-shaped busbar of GIS, which is specially designed and manufactured for experimental research work on partial discharge monitoring in a GIS system to the high voltage laboratory of Electrical Engineering Department of Sharif University of Technology. Also for providing the necessary support for the third author during his post-doctoral study, in which this research work is carried out.

Credit Authorship Contribution Statement

Reza Rostaminia: Conceptualization, Data curation, Formal analysis, Investigation, Methodology, Project administration, Resources, Software, Supervision, Validation, Visualization, Roles/Writing - original draft, Writing - review & editing. **Mehdi Vakilian:** Investigation, Supervision, Validation, Visualization, Writing - review & editing. **Keyvan Firouzi:** Data curation, Supervision, Validation, Visualization, Writing - review & editing.

Declaration Of Competing Interest

The authors declare that they have no known competing financial interests or personal relationships that could have appeared to influence the work reported in this paper. The ethical issues; including plagiarism, informed consent, misconduct, data fabrication and/or falsification, double publication and/or submission, redundancy has been completely observed by the authors.

References

[1] H. Wang, H. E. Jo, and S. J. Kim, "Measurement and analysis of partial discharges in SF6 gas under HVDC," *Meas. J. Int. Meas. Confed.*, vol. 91, pp. 351–359, 2016.

[2] Y. Khan, A. A. Khan, and F. N. A. Budiman, "Partial discharge pattern analysis using support vector machine to estimate size and position of metallic particle adhering to spacer in GIS," *Electr. Power Syst. Res.*, vol. 116, pp. 391–398, 2014.

[3] D. Lim, and S. Bae, "Study on oxygen / nitrogen gas mixtures for the surface insulation performance in gas insulated switchgear," *IEEE Trans. Dielectr. Electr. Insul.*, vol. 22, no. 3, pp. 1567–1576, 2015.

[4] H. X. Ji, L. Cheng-rong, and P. Zhi-kai, "Influence of tip corona of free particle on PD patterns in GIS," *IEEE Trans. Dielectr. Electr. Insul.*, vol. 24, no. 1, pp. 259–267, 2017.

[5] M. Ren, M. Dong, and J. Liu, "Statistical analysis of partial discharges in SF6 gas via optical detection in various spectral ranges," *Energies*, vol. 9, no. 3, p. 152, 2016.

[6] D. Dai, X. Wang, J. Long, M. Tian, G. Zhu, and J. Zhang, "Feature extraction of GIS partial discharge signal based on S-transform and singular value decomposition," *IET Sci. Measur. Technol., vol. 11, no. 2, pp. 186–193, Mar. 2017.*

[7] IEC Standard, "High-voltage test techniques - Partial discharge measurements," IEC 60270, 2001.

[8] A. Bargigia, W. Koltunowicz, and A. Pigin, "Detection of partial discharges in gas insulated substations," *IEEE Trans. Power Deliv.*, vol. 7, no. 3, pp. 1239–1249, 1992.

[9] I. M. Welch, O. Farish, B. F. Hampton, and D. Templeton, "Partial discharge diagnostics for gas insulated substations," *IEEE Trans. Dielectr. Electr. Insul.*, vol. 2, no. 5, pp. 893–905, 1995.

[10] V. M. Ibrahim, Z. Abdul-Malek, and N. A. Muhamad, "Status review on gas insulated switchgear partial discharge diagnostic technique for preventive maintenance," Indonesian Journal of Electrical Engineering and Computer Science, vol. 7, no. 1, pp. 9–17, 2017.

[11] H. Okubo, and A. Beroual, "Recent trend and future perspectives in electrical insulation techniques in relation to sulfur hexafluoride (SF6) substitutes for high voltage electric power equipment," *IEEE Elec. Insul. Mag.*, vol. 27, no. 2, pp. 34–42, 2011.

[12] L. E. Lundgaard, M. Runde, and B. Skyberg, "Acoustic diagnosis of gas insulated substations: a theoretical and experimental basis," *IEEE Trans. Power Deliv.*, vol. 5, no. 4, pp. 1751–1759, 1990.

[13] S. Yoshida, H. Kojima, N. Hayakawa, F. Endo, and H. Okubo, "Light emission spectrum depending on propagation of partial discharge in SF6," in *Conference Record of IEEE International Symposium on Electrical Insulation*, 2008, pp. 365–368.

[14] Siying Wu, Fuping Zeng, Ju Tang, Qiang Yao, and Yulong Miao, "Triangle fault diagnosis method for SF6 gas-insulated equipment", *IEEE Trans. Power Deliv.*, vol. 34, no. 4, 2019, pp 1470-1477.

[15] S. Okabe, S. Kaneko, T. Minagawa, and C. Nishida, "Detecting characteristics of SF6 decomposed gas sensor for insulation diagnosis on gas insulated

switchgears," *IEEE Trans. Dielectr. Electr. Insul.*, vol. 15, no. 1, pp. 251–258, 2008.

[16] Y. Xu, W. Liu, and W. Gao, "Investigation of disc-type sensors using the UHF method to detect partial discharge in GIS," *IEEE Trans. Dielectr. Electr. Insul.*, vol. 22, no. 5, pp. 3019–3027, 2015.

[17] K. Khotimah, U. Khayam, and Y. Suwarno, Tai, M. Kozako, and M. Hikita, "Design of dipole antenna model for partial discharge detection in GIS," in *2015 International Conference on Electrical Engineering and Informatics (ICEEI)*, 2015, pp. 186–191.

[18] W. Gao, D. Ding, W. Liu, and X. Huang, "Analysis of the intrinsic characteristics of the partial discharge induced by typical defects in GIS," *IEEE Trans. Dielectr. Electr. Insul.*, vol. 20, no. 3, pp. 782–790, 2013.

[19] S. Okabe, and S. Kaneko, "Electromagnetic wave propagation in a coaxial pipe GIS model," *IEEE Trans. Dielectr. Electr. Insul.*, vol. 14, no. 5, pp. 1161–1169, 2007.

[20] W. Gao, D. Ding, W. Liu, and X. Huang, "Propagation attenuation properties of partial discharge in typical in-field GIS structures," *IEEE Trans. Power Deliv.*, vol. 28, no. 4, pp. 2540– 2549, 2013.

[21] Q. Li, et al, "Influence of GIS structure on propagation of electromagnetic waves of partial discharge," in *PEAM 2011 - Proceedings: 2011 IEEE Power Engineering and Automation Conference*, 2011, vol. 2, pp. 128–135.

[22] F. Álvarez, F. Garnacho, J. Ortego, and M. Á. Sánchez-Urán, "Application of HFCT and UHF sensors in on-line partial discharge measurements for insulation diagnosis of high voltage equipment," *Sensors (Switzerland)*, vol. 15, no. 4, pp. 7360–7387, 2015.

[23] S. Das and P. Purkait, "Φ-q-n pattern analysis for understanding partial discharge phenomena in narrow voids," in *IEEE Power and Energy Society 2008 General Meeting: Conversion and Delivery of Electrical Energy in the 21st Century*, PES, 2008.

[24] R. Rostaminia, M. Saniei, M. Vakilian, S. S. Mortazavi, and V. Parvin, "Accurate power transformer PD pattern recognition via its model," *IET Science, Measurement & Technology*, vol. 10, no. 7, pp. 745-753, 2016.

[25] L. Li-Xue, H. Cheng-Jun, Z. Yi, and J. Xiu-Chen, "Partial discharge diagnosis on GIS based on envelope detection," WSEAS Transactions on Systems, vol. 7, no. 11, pp 1238-1247, 2008.

[26] L. Li, J. Tang, and Y. L. Liu, "Partial discharge recognition in gas insulated switchgear based on multi-information fusion," *IEEE Transactions on Dielectrics and Electrical Insulation*, vol. 22, no. 2, pp 1080-1087, 2015.

[27] G. Li, M. Rong, X. Wang, X. Li, and Y. Li, "Partial discharge patterns recognition with deep convolutional neural networks," in *2016 International Conference on Condition Monitoring and Diagnosis*, Xi'an, China, 2016, pp 324-327.

[28] F. Bin, F. Wang, Q. Sun , S Chen, J. Fan, and H. Ye, "Identification of ultra high-frequency PD signals in gas-insulated switchgear based on moment features considering electromagnetic mode", *High Volt.*, vol. 5, no. 6, pp. 688-696, 2020.

[29] H. Guo, F. Lu, and K. F. Ren, "Simulation and measurement of PD induced electromagnetic wave leakage in GIS with metal belt," *IEEE Trans. Dielectr. Electr. Insul.*, vol. 21, no. 4, pp. 1942-1949, 2014.

[30] H. Guo, H. Qiu, L. Yao, F. Huang, and K. F. Ren, "Investigation on polarization characteristics of PD-induced electromagnetic wave leakage in GIS with metal belt," *IEEE Trans. Dielectr. Electr. Insul.*, vol. 23, no. 3, pp. 1475-1481, Jun. 2016.

[31] S. Kaneko, S. Okabe, M. Yoshimura, H. Muto, C. Nishida, and M. Kamei, "Detecting characteristics of various type antennas on partial discharge electromagnetic wave radiating through insulating spacer in gas insulated switchgear," *IEEE Trans. Dielectr. Electr. Insul.*, vol. 16, no. 5, pp. 1462-1472, 2009.

[32] Y. Wang, Z. Wang, and J. Li, "UHF Moore fractal antennas for online GIS PD detection," *IEEE Antennas Wireless Propag. Lett.*, vol. 16, pp. 852-855, 2016.

[33] T. Ju, X. Zhongrong, Z. Xiaoxing, and S. Caixin, "GIS partial discharge quantitative measurements using UHF microstrip antenna sensors," in *Proc. 2007 Annual Report - Conference on Electrical Insulation and Dielectric Phenomena*, Vancouver, BC, Canada, Oct. 2007, pp. 116-119.

[34] R. Rostaminia, M. Vakilian, and K. Firouzi, "Influence of gas insulated switchgear configuration components on UHF PD signals," *Journal of Applied Research in Electrical Engineering*, vol. 1, no. 2, pp. 139-148, 2022.

[35] R. Candela, G. Mirelli, R. Schifani, "PD recognition by means of statistical and fractal parameters and a neural network," *IEEE Trans Dielectr Electr Insul.*, vol. 7, no. 1, pp.87-94, 2000.

BIOGRAPHY

Reza Rostaminia received the B.Sc. degree in Electrical and Electronics Engineering from Babol Noshirvani University of Technology, Babol, Iran in 2007, The M.Sc. degree in Electrical Power Engineering from Khaje Nasir Toosi University of Technology (KNTU), Tehran, Iran in 2011 and the Ph.D. degree in Electric Power Engineering (High Voltage Engineering) from Shahid Chamran University of Ahwaz, Ahwaz, Iran in 2017. He was a post-doctoral researcher at the same university from 2019 to 2020. From 2015 to 2018, he was a sabbatical study in Electric Power Engineering (High Voltage Engineering) from Sharif University of Technology, Tehran, Iran in 2021. He joined the Parsian Substation Development Company, Tehran, Iran, where he is currently Technical Head of HV Substation Equipment Department. His research interest is High Voltage Engineering, Dielectrics and Insulation, Partial Discharge, Condition Monitoring and

Diagnosis of High Voltage Equipment, High Voltage Substation Design and Earthing design.

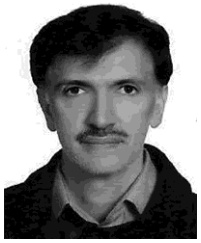

Mehdi Vakilian (M'88–SM'15) received the B.Sc. degree in electrical engineering and the M.Sc. degree in electric power engineering from the Sharif University of Technology, Tehran, Iran, in 1978 and 1986, respectively, and the Ph.D. degree in electric power engineering from Rensselaer Polytechnic Institute, Troy, NY, USA, in 1993. From 1981 to 1983, he was with Iran Generation and Transmission Company, and then with the Iranian Ministry of Energy from 1984 to 1985. Since 1986, he has been with the Faculty of the Department of Electrical Engineering, Sharif University of Technology. During 2001–2003, and 2014-2018 he was the Chairman of the department. During 2003 to 2004, and part of 2007, he was on leave of study at the School of Electrical Engineering and Telecommunications, University of New South Wales, Sydney, Australia. His research interests include transient modeling of power system equipment, especially power transformers, optimum design of high-voltage equipment insulation, monitoring of power system equipment and their insulations, especially with partial discharge measurement, power system transients, and distribution system studies.

Keyvan Firuzi received the B.Sc. degree in Electrical and Electronics Engineering from University of Tabriz, Tabriz, Iran in 2012, The M.Sc. degree in Electrical Power Engineering and the Ph.D. degree in Electric Power Engineering (High Voltage Engineering) from Sharif University of Technology, Tehran, Iran in 2014 and 2019 respectively. He was a post-doctoral researcher at the same university from 2019 to 2020. From 2015 to 2018, he was a Research Scientist with Niroo Research Institution (NRI). In 2021, he joined the Electrical and Electronics Engineering Department at METU, where he is currently working as an Assistant Professor. His research interest is High Voltage Engineering, Dielectrics and Insulation, Partial Discharge, Condition Monitoring and Diagnosis of High Voltage Equipment, Signal Processing, and Machine Learning.